01 Jun 2016

Design of Magnesium Phosphate Cement Based Composite for High Performance Bipolar Plate of Fuel Cells

Wenbin Hao

Hongyan Ma
Missouri University of Science and Technology, mahon@mst.edu

Zeyu Lu

Guoxing Sun

et. al. For a complete list of authors, see https://scholarsmine.mst.edu/civarc_enveng_facwork/708

Recommended Citation

W. Hao et al., "Design of Magnesium Phosphate Cement Based Composite for High Performance Bipolar Plate of Fuel Cells," *RSC Advances*, vol. 6, no. 61, pp. 56711-56720, Royal Society of Chemistry, Jun 2016. The definitive version is available at https://doi.org/10.1039/c6ra11573j

RSC Advances

PAPER

View Article Online
View Journal | View Issue

Cite this: *RSC Adv.*, 2016, **6**, 56711

Design of magnesium phosphate cement based composite for high performance bipolar plate of fuel cells

Wenbin Hao,[a] Hongyan Ma,*[ab] Zeyu Lu,[a] Guoxing Sun[a] and Zongjin Li[a]

Received 4th May 2016
Accepted 8th June 2016

DOI: 10.1039/c6ra11573j

www.rsc.org/advances

In this work, we report a comprehensive study on a magnesium phosphate cement (MPC) based composite as the construction material for high performance bipolar plates of fuel cells. MPC with partial replacement of fly ash was employed as the binding matrix. Some carbon-based materials, such as graphite, carbon black, carbon fiber, and multi-walled carbon nanotubes were used to construct the conductive phase. A simple hot-press process was applied to produce the composite. The formula and the structure of the composite was modified and adjusted to optimize the properties of the composite to meet the US DOE 2015 technical targets, including the introducing of a reinforcement support. Finally, all the technical targets such as electrical conductivity (>100 S cm^{-1}), the flexural strength (>25 MPa), the corrosion resistance (<1 μA cm^{-2}), and gas permeability (<10^{-5} cm^3 (s cm^2)$^{-1}$) were achieved as well as low cost (<5 $ per kW). The optimized formula and the detailed procedures to fabricate the MPC based composite were concluded.

1. Introduction

Fuel cells, especially PEMFC (proton exchange membrane fuel cells), due to their multifaceted advantages, are one of the most promising alternative technologies for power generation.[1] In practical applications, hundreds or thousands of single cells are assembled as stacks to achieve scalable power supply (from 10 kW to 1 MW). Bipolar plates (BP) are one of the key components of fuel cell stacks, which account for around 80% of the volume and 45–60% of the stack cost.[2–4] Traditional BP materials include graphite, metals and polymeric composites. High cost and techniques limitations of those materials confine the commercialization of fuel cell stacks.[5] While graphite is a material for BP due to its ultrahigh electrical conductivity.[6] However, the fabrication cost of making graphite BP remains high due to its brittleness, which results in difficulties in mechanical processing of flow-field. Though the metallic BP has high electrical conductivity and excellent mechanical properties as well as low fabrication cost, it is easily corroded in acidic environment of fuel cell anode, which severely shortens the service life of such BP.[3,5,7] Anti-corrosion coatings have been applied on the surface of metallic BP to enhance the corrosion resistance.[8] US patent No. 7632592 B2 discloses a method of applying a high-grade stainless steel or an alloy corrosion-resistant coating on a low-grade stainless steel (304L or 316L) substrate plate by a kinetic spray process.[9] US patent No. 6372376 B1 discloses a method to enhance the corrosion resistance by providing a corrosion-resistant polymer coating containing plurality of electrically conductive, corrosion-resistant particles on the metallic substrate.[10] Though the corrosion resistance is enhanced, these methods increase the cost and/or decrease the BP's conductivity by increasing the contacting resistance between the coating and the substrate. A number of polymer/carbon fillers composites have also been developed as BP materials. US patent No. 7910040 B2 discloses a method to prepare a composite BP using a bulk molding compound process.[11] In that BP, vinyl ester works as binder and graphite powder, carbon nanotubes (CNTs), carbon fiber, and modified organo clay work as conductive fillers. Taherian *et al.* developed a sandwich-structured triple-filler composite BP consisting of phenolic resin, graphite powder, expanded graphite, carbon fiber, and thin carbon fiber cloth.[12] However, the electrical conductivity and flexural strength of the polymer/carbon filler composite still could not be well balanced. Researchers in Wuhan University of Technology developed an aluminate cement-graphite powder composite BP, which has been proven to be high-strength, highly conductive with low-cost.[13,14] However, the structure of aluminate cement becomes unstable in acidic environment (<4 pH), accompanied by the dissolution of metallic ions (such as Ca^{2+}, Al^{3+}, *etc.*), which will contaminate the proton exchange membrane and affect the performance of PEMFC. Nowadays, researchers financially supported by US department of energy (DOE) are yet struggling

[a]*Department of Civil and Environmental Engineering, Hong Kong University of Science and Technology, Clear Water Bay, Kowloon, Hong Kong, China*

[b]*Department of Civil, Architectural and Environmental Engineering, Missouri University of Science and Technology, Rolla, MO 65401, USA. E-mail: mahon@mst.edu; Tel: +1-573-341-6250*

Table 1 The main targets of US DOE 2015 for bipolar plate

Parameter	Units	DOE target 2015
Cost	$ per kW	5
Electrical conductivity	S cm^{-1}	>100
Flexural strength	MPa	>25
Corrosion current density	μA cm^{-2}	<1
Gas permeability	cm^3 ($s\ cm^2$)$^{-1}$	$<10^{-5}$

to achieve the US DOE 2015 technical and cost targets of the BP. The main targets of US DOE 2015 are listed in Table 1.[15]

Magnesium phosphate cement (MPC) is a kind of low-pH cement, which can keep stable under acidic environment.[16,17] When using MPC as the matrix and carbon-based materials (graphite powder, carbon fiber, carbon nanotubes, *etc.*) as fillers, it is possible to produce high performance BP that fulfills all technical targets of US DOE 2015 and simultaneously achieves low cost.

In this work, we report a comprehensive study on the MPC based composite as the construction material for BP. MPC with certain amount replacement of fly ash was used as the binding matrix. Carbon-based materials including graphite, carbon black, carbon fiber, and carbon nanotubes were applied as the conductive fillers. The composite was fabricated using a hot-press process. During the characterization of the composite, modifications of formula and structure of the composite were applied to reach the technical targets, including the introducing of a reinforcement support. Finally, all the technical targets of the US DOE 2015, including electrical conductivity, the flexural strength, and the corrosion resistance *etc.* are achieved as well as low cost.

2. Materials and methods

2.1. Raw materials

The raw materials used in this study comprise materials for making MPC, carbon fillers for enhancing the electrical conductivity, and supplementary materials for achieving higher flexural strength and enhancing the corrosion resistance. The scanning electron microscopy (SEM) images of the raw materials are shown in Fig. 1.

Raw materials with reinforcing materials for making MPC include dead burnt magnesia powder (calcined under 1600 °C for 5 hours) with a purity of 95.1%, potassium dihydrogen phosphate (KDP) powder (chemical reagent), fly ash (FA) and deionized water. The magnesia powder (passed a 300 μm sieve) was supplied by Jinan Magnesia-Carbon Brick Plant Co. Ltd., Shandong, China; the KDP powder (passed a sieve with the pore size of 250 μm) was supplied by Guangzhou Chemical Reagent Factory, Guangdong, China; and the FA (with a mean particle size of 18 μm) was supplied by China Light and Power Co. Ltd., Hong Kong. The composition of the dead burnt magnesia and FA were listed in Table 2. Carbon fillers were micro-sized powder graphite (with particles smaller than 30 μm > 95%), nano-sized powder carbon black (CB) (mean particle size < 100 nm), short carbon fiber (CF) (2 mm pitched carbon fiber), and industrial multi-walled carbon nanotubes (MW-CNTs).

2.2. Fabrication of the MPC based composite

Blending and hot-press were employed to fabricate the MPC based composite.[11,17] The dead burnt magnesia, KDP powder and certain amounts of FA and carbon fillers were dry mixed at room temperature (RT). The M/P ratio was fixed to be 8.[18] Volume replacements of 10–50% in the solid phases with FA and/or graphite were investigated in this study. The volume replacements of 0–10% and 0–8% in addition to graphite with carbon black and carbon fiber were applied in the study, respectively. 0–4% of MW-CNTs was added to adjust the formulae. After dry mixing of the solids, deionized water was added to initiate the hydration reaction. The water/cement ratio was fixed to be 0.25.[19] The wet cement paste was stirred vigorously at RT for 30 min. The acquired paste was put in the die mold (65 mm × 65 mm), and pre-pressed under 2 ton loads in the hot-press machine at 60 °C for 10 min. Then, the load was increased to 10–40 ton and the paste was hot-pressed at 60–140 °C for another 5–60 min. After that, the load was reduced to 2 ton again and the machine temperature was decreased to RT through air cooler. Finally, the MPC based composite was obtained after releasing from the mold.

2.3. Characterizations on the MPC based composite

2.3.1. Microstructure analysis. The SEM images were acquired to investigate the morphology information of the MPC based composite specimens *via* JEOL 6390 (JEOL Ltd., Japan). The elemental distributions in the specimens were also investigated *via* EDAX in mapping mode.

2.3.2. Measurement of electrical conductivity. A high-precision four-point conductivity probe (SX1944, Shanghai Yanhua Ltd., China) was used to measure the electrical resistivity. During the measurements, the probe was attached to the specimen surface. A certain voltage (V) was applied to the probe to generate a current (I). Then, the electrical resistivity (ρ) was calculated as:

$$\rho = CV/I \quad (1)$$

where C is a constant related to the probe, which is equal to 2π in our test system. The electrical conductivity was the reciprocal of the electrical resistivity. The average electrical conductivity of each specimen was obtained from 18 repeated measurements at different locations of the specimen.

2.3.3. Measurement of flexural strength. A three-point bending test was conducted following the procedure prescribed by ASTM C78/C78 M-10 (MTS 858 Universal Testing Machine, MTS, MN, USA). For each formula, 3 specimens with width of 50 mm and thickness of 3 mm were measured using a span of 80 mm and a stroke control at a loading rate of 0.1 mm min^{-1}. Two linear variable differential transformers (LVDTs) were set up on each side of the specimen to measure the mid-point deflection.

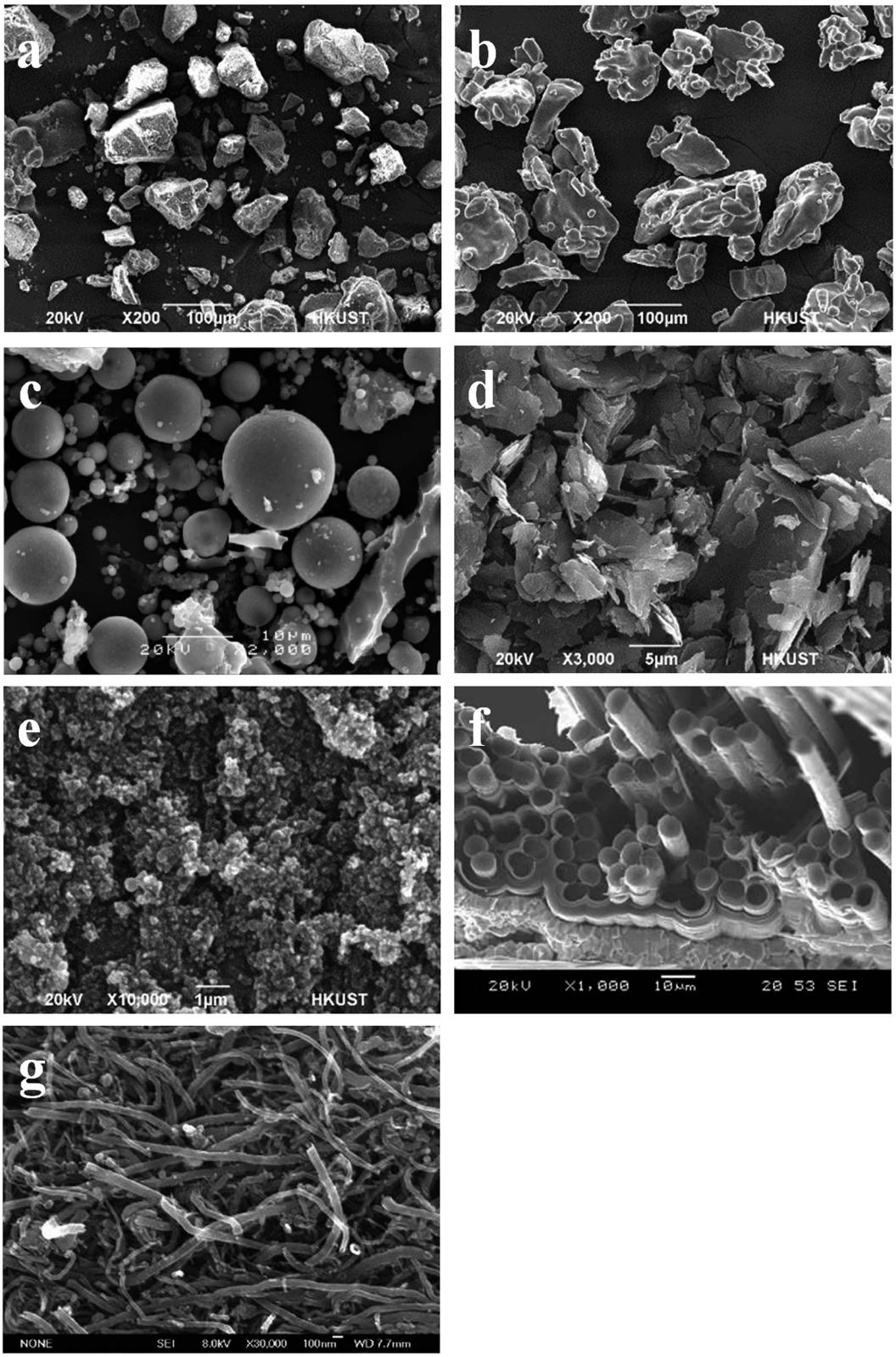

Fig. 1 SEM images of main raw materials composed of the MPC based composite: (a) magnesia, (b) potassium dihydrogen phosphate, (c) fly ash, (d) graphite, (e) carbon black, (f) carbon fiber, and (g) multi-walled carbon nanotubes.

2.3.4. Measurement of corrosion resistance. The corrosion resistance of the MPC based composite was measured *via* an electrochemical working station equipped with a current amplifier (CHI 660E&680, Shanghai CHI, China). The typical three-electrode system was employed in the electrochemical characterizations, in which a MPC based composite plate used

Table 2 Chemical compositions of the dead burnt magnesia and fly ash (wt%)

Materials	CaO	SiO_2	Al_2O_3	Fe_2O_3	MgO	SO_3	K_2O	Other minors	LOI[a]
Magnesia	1.32	3.22	—	0.27	95.1	—	—	0.09	—
Fly ash	4.73	60.57	21.95	1.71	2.04	1.18	0.62	4.08	3.12

[a] LOI: loss on ignition.

as the working electrode, a standard Ag/AgCl electrode as the reference electrode, and a platinum sheet as the counter electrode. The specimen dimension of 10 mm × 10 mm was used during the measurements of Tafel technique. Tafel plots were drawn to determine the corrosion current density.

2.3.5. Measurement of gas permeability. When the aforementioned key properties were fulfilled, the composition of the MPC based composite was determined. Then, the gas permeability of such composite was assessed indirectly *via* the porosity measurement. Mercury intrusion porosimetry (MIP) technique was employed to investigate the pore structures of the MPC based composite. The cuboids with the smallest dimension of 5–8 mm were sawed from the specimens of MPC based composite. Then, the samples were obtained after a solvent replacement drying procedure was applied to the cuboids. A Micromeritics AutoPore IV 9500 (Micromeritics Instrument Corporation, Norcross, GA, USA) was used for MIP measurements, and the maximum pressure that could be applied was 30 500 psi (210 MPa). The obtained results were compared to that of cast MPC paste with same drying pre-treatment.

3. Results and discussion

3.1. Microstructure analysis

The SEM images with elemental distributions in the mapping mode of the MPC based composites are shown in Fig. 2. In the figure, a dense morphology was observed on the surface of the MPC based composite, which might provide low gas permeability through the material.[17] It could also be seen in the figure that the binder phase-the magnesium potassium phosphate (MKP) phase of hydration product was well formed to connect all the components and flake-shaped graphite particles were well distributed in the composite. No carbon fillers presented in the binder phase, indicating that the binder phase was electrically insulated. However, when carbon fillers are incorporated into the binder matrix with enough high volume fractions, it is expected that they can connect to each other and percolate through the material, so that the composite can be electrically conductive.

In the images of mapping mode shown in Fig. 2, it can be seen that the carbon phase (mainly carbon fillers, such as graphite) was well connected and percolated through the MKP phase continuously, suggesting the formation of the electrical conductive network. Also, in the images of mapping mode shown in Fig. 2a, unreacted magnesia particles were observed in the carbon-free regions, which indicated the existence of poorly crystallized MKP phase. The uniform distribution of K and P in the images of mapping mode could be attributed, to some extent, to the existence of the dissolved but unreacted KDP. The SEM observation indicated that poorly crystallized MKP-bonded graphite flakes percolated through the whole composite to provide the electrically conductive pathways, and unreacted

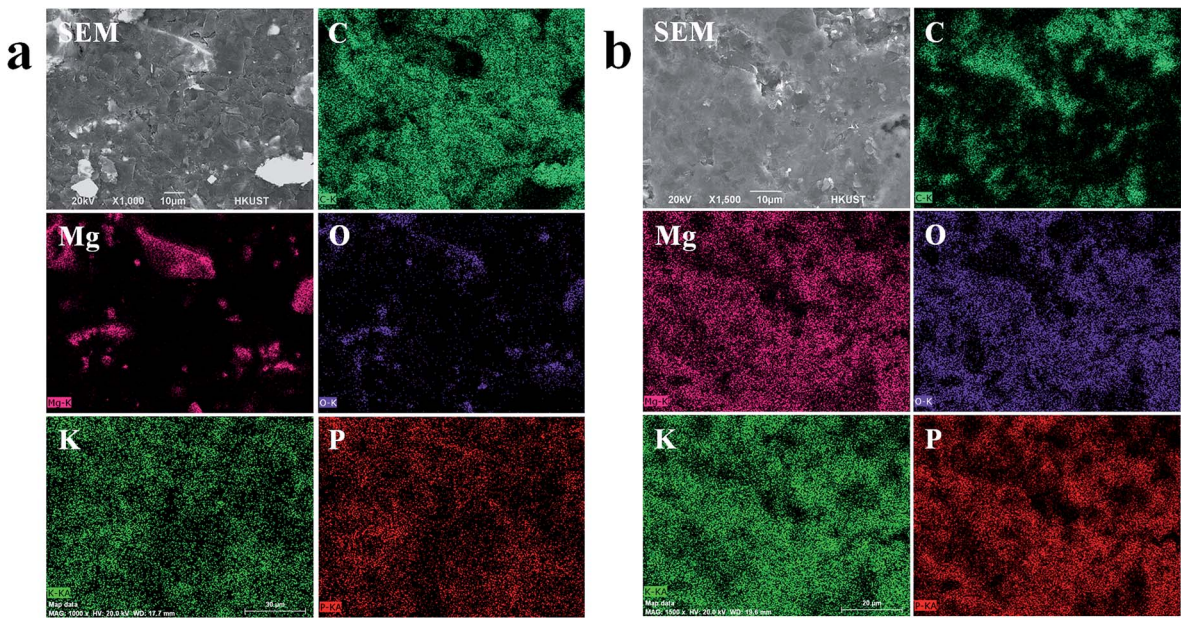

Fig. 2 SEM images with elemental distributions in the mapping mode of the MPC based composite: (a) bulk and (b) surface.

magnesia particles and sometimes large MKP particles brought in homogeneity to make the conductive pathway more tortuous.

3.2. Electrical conductivity

Effects of different carbon fillers and filler combinations with different volume fractions on the electrical conductivity of the MPC based composites are reported in this part. In light of the optimized hot-press parameters, the evolution of electrical conductivity of composite with a binder M/P of 8, including the volume fraction effects of graphite, CB, CF, and MW-CNTs, is shown in Fig. 3. According to the results in Fig. 3a, the target electrical conductivity (100 S cm^{-1}, the target conductivity of BP in US DOE 2015) could be achieved at the volume fraction of 43%, when graphite powder was used as mono-filler. As a high graphite volume fraction might impact the properties like flexural strength and corrosion resistance, other high-conductivity fillers were used in addition to graphite, to achieve the target electrical conductivity at a relatively low graphite volume fraction.[14,20]

Fig. 3b shows that using CB as carbon filler could significantly raise the electrical conductivity and the target electrical conductivity was achieved at an overall carbon volume fraction of 35%. The prominent role of CB in raising electrical conductivity should be attributed to its filling and bridging effects. The nano-sized CB particles packed in and bridged the micro-sized graphite flakes to enhance the electrical connectivity. Although the incorporation of CB at low volume fraction in addition to graphite can significantly enhance the electrical conductivity, it also led to a significant increase of corrosion current density at the same time, meaning a worse corrosion resistance. The reasons resulting in this drawback would be discussed in the part of corrosion resistance results.

CF was also expected to enhance the electrical conductivity, but the filling effect was limited as it is a micro-sized material. The effect of CF, additional to 30% graphite, on electrical conductivity is plotted in Fig. 3c. It can be seen that certain aspect ratio of CF (~5%) helped the connection of graphite flakes and reduced the tortuosity of the conductive pathways. The target conductivity was also achieved at an overall carbon volume fraction of about 35%. However, further increase of CF would lead to a sharp decrease of electrical conductivity. This decrease was due to the poor dispersion of CF in the composite matrix, for instance, CF conglomerate when its volume fraction is too high, which destroys the connections in the composite and generates lots of defects and uncontinuities. Therefore, compared with CB, CF was low-fraction effective filler.

MW-CNTs, having large aspect ratio as one-dimensional nano-sized but overall micro-sized carbon material, were thus expected to be more effective than both CB and CF as carbon filler. In addition, MW-CNTs may also enhance flexural strength due to its high strength properties. Based on a reference formula: M/P = 8, W/C = 0.25, graphite 40%, CF 1%, and a FA replacement ratio of 30%, MW-CNTs were added as carbon

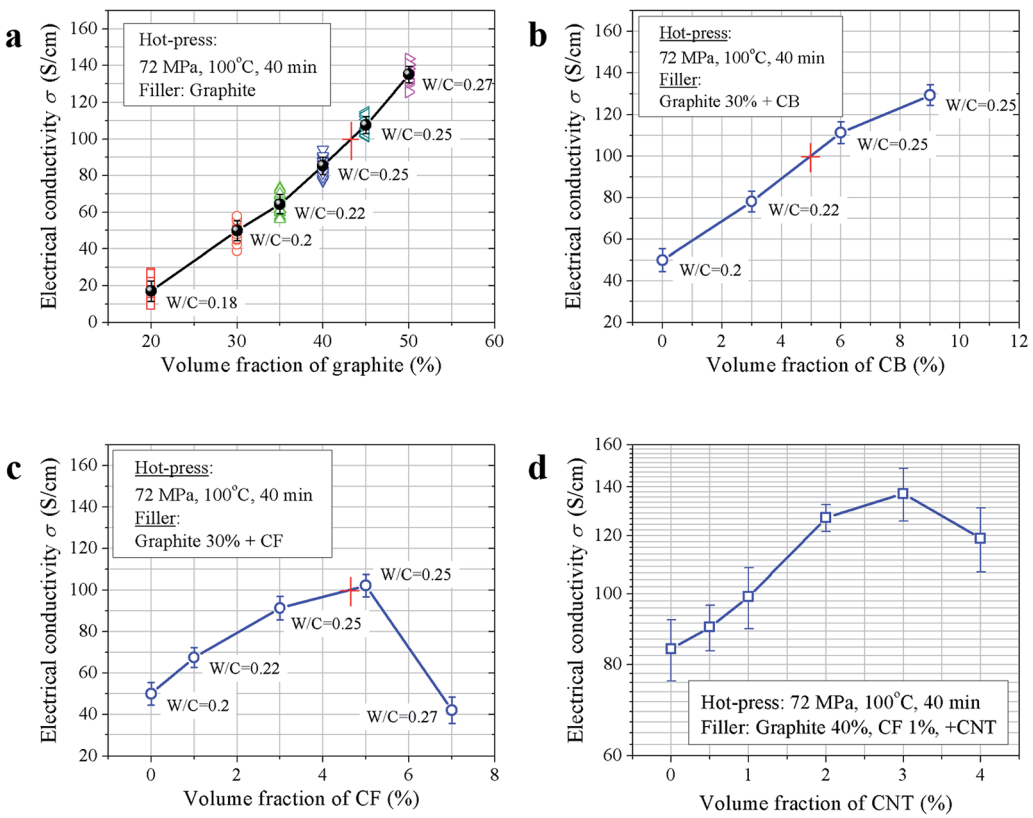

Fig. 3 Electrical conductivity of MPC based composite as a function of the carbon filler volume fractions: (a) graphite, (b) carbon black (CB), (c) carbon fiber (CF), and (d) multi-walled carbon nanotubes (MW-CNTs).

filler. The influence of the addition of MW-CNTs on the electrical conductivity is shown in Fig. 3d. It can be seen that an addition of MW-CNTs up to 3%, in addition to 40% graphite, could increase the electrical conductivity. The target electrical conductivity was achieved when the addition of MW-CNTs was higher than 1%. However, the rising curve showed a turning point at the MW-CNTs amount of 3%. Beyond that point, the extra amount of MW-CNTs would cause the drop of electrical conductivity. Similar to CF, MW-CNTs were also a kind of large aspect ratio material which can act as bridges between graphite particles. This bridging effect was reflected by the positive effect of MW-CNTs on the composite conductivity at low volume fraction. In this situation, the isolated graphite particles connected with each other more tightly by the MW-CNTs. When the volume fraction is relatively high, MW-CNTs are easily agglomerate causing poor dispersion of MW-CNTs in the MPC–graphite matrix. The conglomeration of MW-CNTs can even reduce the effectiveness of hot-press, and loosen the composite structure. In such a case, the incorporation of MW-CNTs will break the interconnections between graphite particles rather than bridge them. The negative effect of MW-CNTs at relatively high amounts should be attributed to such mechanisms.

In summary, the higher content of graphite would benefit the electrical conductivity of the MPC based composite. In addition, a slight amount of carbon fillers, such as CB, CF, or MW-CNTs could significantly increase the electrical conductivity of the MPC based composite and reduce the volume fractions of total carbon in the composite at the same time. As a result, the observed proper amount of CB, CF, and MW-CNTs to achieve the target electrical conductivity of the composite (100 S cm^{-1}) were 5%, ~5% and 2–4%, respectively.

3.3. Flexural strength

Effects of different carbon fillers and filler combinations at different volume fractions on the flexural strength of the MPC–carbon composites are reported here. The influences of graphite volume fractions, as well as the incorporations of CB and CF in addition to 30% graphite powder, and the influence of MW-CNTs volume fractions on the flexural strength of composite, are shown in Fig. 4. It suggested that increasing graphite volume fractions led to the decrease of volume fraction of the binder phase, which resulted in the decrease of the flexural strength accordingly. Especially, when the graphite volume fraction exceeded 20%-the percolation threshold, cracks occurring in loading could propagate much easier along the filler–binder interfaces and lead to rupture, thus the flexural strength decreased sharply.[13]

The effect of CB in addition to graphite on the flexural strength of the MPC–graphite–CB binary carbon filler composite is shown in Fig. 4b, which indicates that flexural

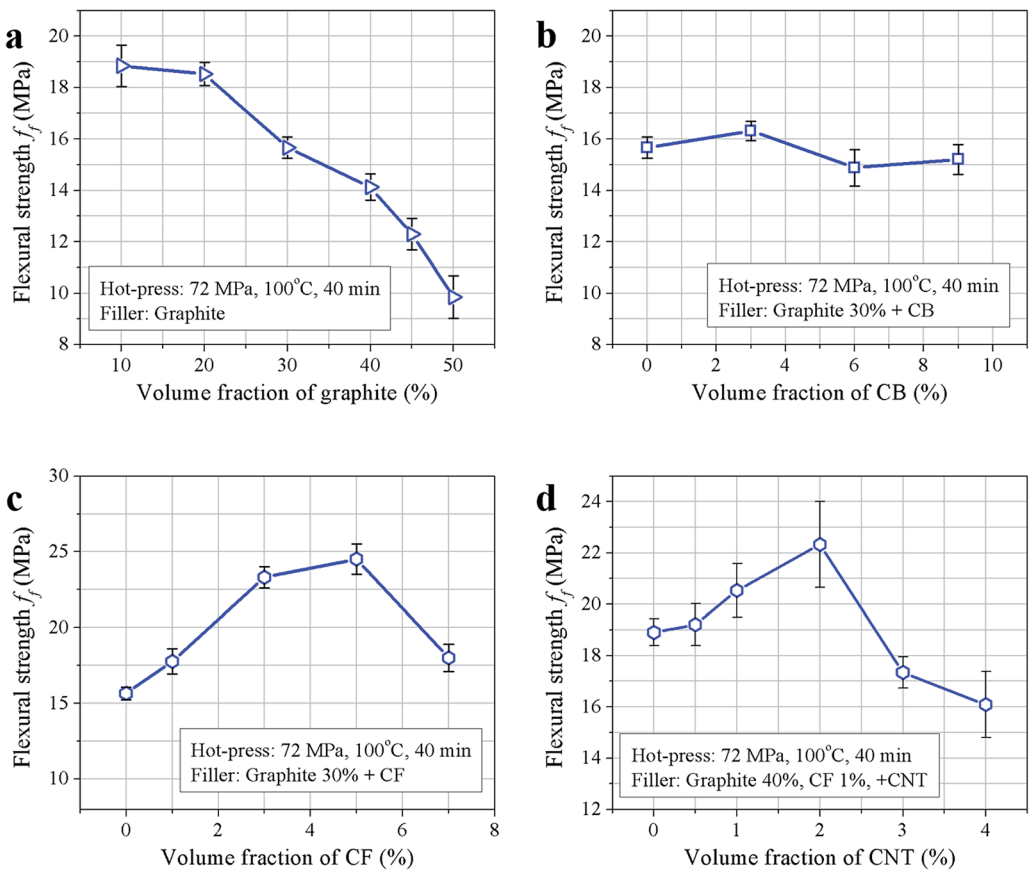

Fig. 4 Flexural strength of MPC based composite as a function of the carbon filler volume fractions: (a) graphite, (b) carbon black (CB), (c) carbon fiber (CF), and (d) multi-walled carbon nanotubes (MW-CNTs).

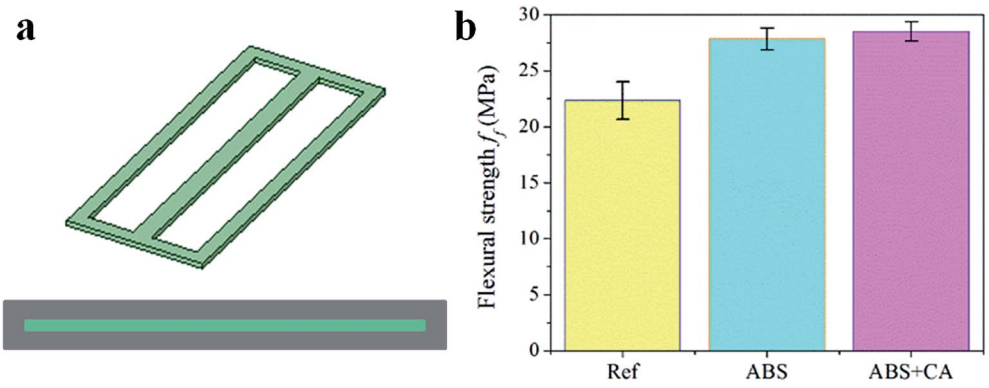

Fig. 5 Schematic view of ABS net and ABS net embedded MPC based composite plate (a), influence of ABS net and CA on the flexural strength of the resulting MPC based composite plate (b) (ABS: acrylonitrile butadiene styrene co-polymer; CA: coupling agent).

strength fluctuated along the increasing of carbon black volume fractions, and no obvious enhancement or weakening was observed. This phenomenon might be due to the counteractions between the finer replacement effect and the inert aggregate effect of CB, which should increase the flexural strength and decrease the flexural strength, respectively.[21,22]

CF was expected to play a prominent role in raising the flexural strength. As shown in Fig. 4c, in MPC–graphite–CF binary carbon filler composite, the incorporation of small amount of CF, in addition to 30% graphite, increased the flexural strength significantly. The achieved maximum flexural strength (24.3 MPa) approached the target value (25 MPa, the target flexural strength of BP in US DOE 2015) with an overall carbon volume fraction of 35%. Unfortunately, further increase in CF volume led to sharp decrease in flexural strength, owing to the conglomeration of carbon fiber under high volume fraction or high pressure. The ternary carbon filler composite of MPC–graphite 28%–CB 4%–CF 1% with a W/C of 0.25, which fulfilled the electrical conductivity requirement, have also been tested for flexural strength and the measured flexural strength was 20.6 MPa.

The influence of MW-CNTs volume fractions on the flexural strength of the resulting composite, in comparison with a reference composite of (M/P = 8, W/C = 0.25, graphite 40%, CF 1%, and a FA replacement ratio of 30%), is shown in Fig. 4d. A turning point also appeared on this plot (just like that in Fig. 4a), at a MW-CNTs volume fraction of 2%. Before the turning point, the flexural strength increased along with the increasing of MW-CNTs volume fractions, while beyond that the increasing MW-CNTs dosages showed a negative effect on flexural strength. These contradictory effects could be explained by the previously proposed mechanism as well. At low dosages, the nano-sized MW-CNTs facilitated the hydration of MPC, and thus resulted in higher flexural strength. The larger aspect ratio of MW-CNTs also contributed to this positive effect. At high dosages, the agglomeration of MW-CNTs was the main reason of the negative effect on flexural strength. As shown in Fig. 4d, when MW-CNTs volume fraction reached or exceeded 3%, the flexural strength was even lower than the reference composite. As a result, the achieved maximum flexural strength of the MW-CNTs added MPC based composite was 22.6 MPa.

By analogy with the concept of reinforced concrete, a macro-reinforcement should be more effective in improving the flexural strength of brittle material. For the MPC based composite, acrylonitrile butadiene styrene co-polymer (ABS) net was examined for its effectiveness as a macro-reinforcement to improve the flexural strength.[23] In order to meet the target flexural strength of US DOE 2015, surface-rough ABS nets were produced through 3D printing and employed as a macro-reinforcement for the MPC based composite, as shown in Fig. 5a. The thickness of the ABS net used was 0.5 mm, and the size was smaller than the target plate with margins of 8 mm in each side. It should be mentioned the size of the ABS nets could be adjusted to fulfill the manufacturing requirements of MPC based BP. Due to the high flexural strength of ABS and the surface roughness of the net, which could provide good physical bonding, the ABS net reinforced the specimen of MPC based composite and a much higher flexural strength was achieved. A surface treatment on the ABS net using silane coupling agent (CA) could even further enhance the flexural strength due to the additional chemical bonding.[12] As a result, the flexural strength of the resulting MPC based composite plate could be as high as 28 MPa, as shown in Fig. 5b.

3.4. Corrosion resistance

Effects of different carbon fillers and filler combinations of reinforcing material with different volume fractions on the corrosion resistance of the MPC–carbon composites have been studied. The influences of graphite volume fractions, as well as the incorporations of CB and CF in addition to 30% graphite powder, and MW-CNTs in addition to 40% of graphite powder with 30% and 40% replacement of FA on the corrosion resistance of composite, are shown in Fig. 6. It shows the influence of graphite volume fraction on the corrosion resistance of MPC–graphite composite. The corrosion current density increased along with the increase of graphite volume fraction, indicating even worse corrosion resistance. The lessened corrosion resistance could be attributed to the increased sites (or probability) for the access of oxygen atoms to the graphene sheets of graphite flakes. The target corrosion resistance could be guaranteed only when the graphite volume fraction was below 25%, where the

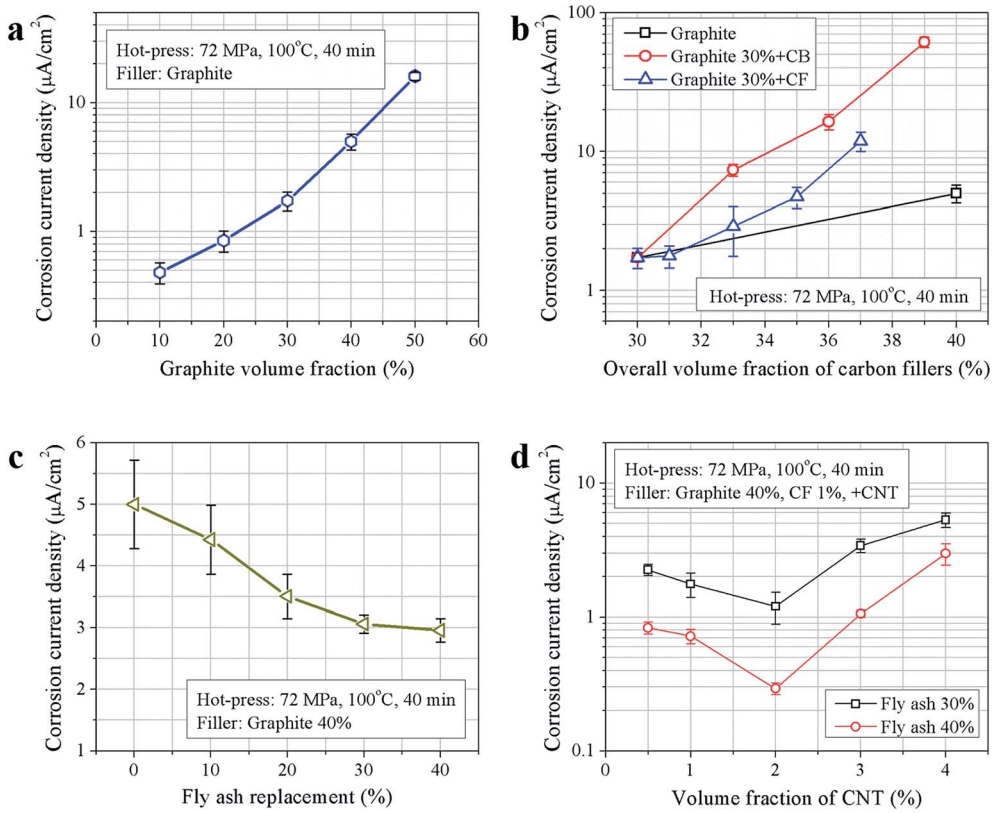

Fig. 6 Corrosion current density of MPC based composite as a function of the carbon filler or fly ash volume fractions: (a) graphite, (b) carbon black (CB) and carbon fiber (CF), (c) fly ash replacement, and (d) multi-walled carbon nanotubes (MW-CNTs) with 30% and 40% fly ash replacement.

required electrical conductivity could not be fulfilled.[13,14] It is a common sense in composite BP that as the electrical conductivity increases the corrosion resistance is expected to reduce.[23] The correct balance between these two properties is a central point to guarantee the long term stability of the composite BP.

Fig. 6b illustrates the effects of CB and CF, additional to 30% graphite, on the composite corrosion resistance. According to the comparison, adding of CB increased the corrosion current density much more significantly than graphite. The deleterious effect of CB could be attributed to its chemical instability, which arises from the presence of numerous dangling bonds and defects.[24] At small amount addition, CF suppressed the negative effect of increasing conductivity on corrosion resistance, compared with graphite. However, addition of CF at relatively high volumes also led to significant lessening of corrosion resistance. Different from CB, the harm brought by CF should not be attributed to its structure, but the agglomeration of CF which generate defects in the composite and expose more sites (or probability) to the potential chemical attack.

Fig. 6c shows a positive effect of FA replacement of magnesia on the corrosion resistance, which was tested based on 40% graphite composite. As mentioned above, the corrosion resistance normally declined as the electrical conductivity increased. This trend would fail when the graphite volume fraction was fixed while MW-CNTs was added to increase the electrical conductivity. The influence of MW-CNTs volume fractions on the corrosion resistance of the resulting composite is shown in Fig. 6d, in comparison with a reference composite of (M/P = 8, W/C = 0.25, graphite 40%, CF 1%, and a FA replacement ratio of 30%). It can be seen that, as the MW-CNTs volume fraction increased up to 2%, in addition to 40% graphite, the corrosion current density decreased to a level very close to the target (1 μA cm^{-2}). This increased corrosion resistance should be attributed to a twofold reason. On one hand, the cylindrical graphene structure of MW-CNTs significantly lowered the probability of oxygen attack, so that corrosion current density did not increase along with the increasing amounts of MW-CNTs. On the other hand, small amount of MW-CNTs, as a nano-structured material, could facilitate the hydration of MPC to achieve a higher degree of hydration. This made the microstructure denser and the exposure opportunity of graphite particles to the acid environment less. However, when the MW-CNTs volume fraction exceeded 2%, the corrosion current density increased sharply. This negative effect could be explained again by the difficulty of MW-CNTs dispersion due to the agglomeration. The agglomeration of MW-CNTs loosened the microstructure of the composite, thus more graphite particles were exposed to the acid environment and oxygen atoms. It's worth noting that corrosion resistance is more sensitive to the MW-CNTs agglomeration compared with electrical conductivity, as shown by the turning points in Fig. 3d and 6d. It is also shown in Fig. 6d that when the FA replacement was increased from 30% to 40%, the corrosion resistance of the

composite could further be improved, as shown by the overall decline of the corrosion current density. The corrosion current density values of most specimens were reduced to a level below the required target (1 μA cm^{-2}), except for the specimen with MW-CNTs at 4.0% dosage. The optimized dosage of MW-CNTs also appeared at 2.0%, which achieved a corrosion current density as low as 0.31 μA cm^{-2}.

3.5. Gas permeability

According to the above mentioned measurements, the best composition of the MPC based composite was M/P = 8, W/C = 0.25, G 40%, CF 1%, MW-CNTs 2%, FA replacement 40%. The porosity of the MPC based composite with such composition was measured *via* the MIP method. The porosity of the cast MPC paste was also measured as the reference. As verified in the literature report, the cast MPC paste is a low permeability material and the typical gas permeability of cast MPC paste is lower than 10^{-8} cm^3 (s cm^2)$^{-1}$.[17,25] Because the composite was formed in a hot-press process, the porosity of the composite was expected to be much lower than the reference MPC paste which was formed by casting, and the pore structure of the composite should be much finer as well. This was proven by the MIP results as shown in Fig. 7. A comparison of the 2nd intrusion curves also indicated that the pore network in the composite was much more tortuous than that in the cast MPC paste, as a much higher fraction of pores were ink-bottle pores. As estimated from Fig. 7, the gas permeability of the composite was more than 2 orders of magnitude lower compared to the cast MPC paste. The gas permeability target of US DOE 2015 was just 10^{-5} cm^3 (s cm^2)$^{-1}$ as for foil BP. Consequently, the MPC based composite fulfilled the gas permeability target congenitally.

3.6. Other properties

The cost of the MPC based composite with an ABS net reinforcement was quite low due to the low cost of raw materials and the density of the MPC based composite was measured to be less than 2 g cm^{-3}. It was estimated that the cost of such composite as construction material for BP was only ~1.5 $ per kW.[15] Thus, the MPC based composite could achieve the cost target of US DOE 2015 (5 $ per kW). The reliably achieved properties of MPC based composite are listed in Table 3. The formula of MPC based composite was [M/P = 8, W/C = 0.25, G 40%, CF 1%, MW-CNTs 2%, FA replacement 40%]. It could be seen that this composite can achieve better electrical conductivity, corrosion resistance, and gas permeability than the targets, except the flexural strength was slightly lower. This slightly lower strength could be overcome by introducing an ABS net as a macro-reinforcement. Finally, all technical targets were achieved.

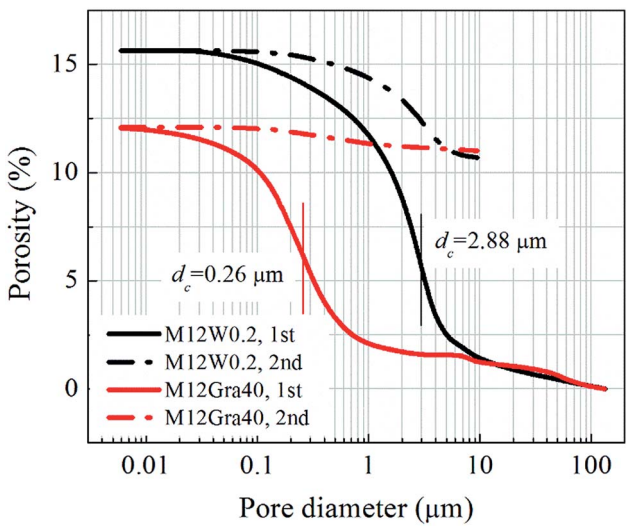

Fig. 7 The pore structures of cast MPC paste (black) and hot-pressed MPC based composite (red).

Table 3 Reliably achieved properties of MPC based composite compared with the DOE 2015 targets

Parameter	Units	Achieved property	DOE 2015 target
Cost	$ per kW	~1.5	5
Electrical conductivity	S cm^{-1}	116	100
Flexural strength	MPa	22.6 (28 *via* reinforcement)	25
Corrosion current density	μA cm^{-2}	0.31	1
Gas permeability	cm^3 (s cm^2)$^{-1}$	$\ll 10^{-5}$	$<10^{-5}$

4. Conclusions

In this work, a comprehensive study on the MPC based composite as the construction material for bipolar plate was conducted. MPC with certain amount replacement of fly ash (FA) was applied as the binding matrix and carbon-based materials including graphite (G), carbon black (CB), carbon fiber (CF), and multi-walled carbon nanotubes (MW-CNTs) were applied as the conductive fillers. After a dry mixing and a short hydration process, the composite was formed *via* a hot-press process. During the characterizations of the composite, the formula was modified and the structure was adjusted in order to achieve all the targets, including the introducing of an ABS net reinforcement support. As a result, the optimized formula of the composite was [M/P = 8, W/C = 0.25, G 40%, CF 1%, MW-CNTs 2%, FA replacement 40%]. Finally, all the technical targets of the US DOE 2015, such as electrical conductivity (116 S cm^{-1}), the flexural strength (28 MPa), the corrosion resistance (0.31 μA cm^{-2}), and gas permeability ($\ll 10^{-5}$ cm^3 (s cm^2)$^{-1}$) were achieved as well as low cost (~1.5 $ per kW).

Acknowledgements

This work received the support from Nano and Advanced Material Institute (NAMI) Limited, Hong Kong. The research fund was applied by NAMI from the Hong Kong Innovation and Technology Fund (HK-ITF) with a project No. of ITP/033/12NP.

The authors also acknowledge the help from the colleagues in Prof. Zongjin Li's group.

References

1 V. Metha and J. S. Cooper, *J. Power Sources*, 2003, **114**, 32–53.
2 W. Qian, D. P. Wilkinson, J. Shen, H. Wang and J. Zhang, *J. Power Sources*, 2006, **154**, 202–213.
3 A. Hermann, T. Chaudhuri and P. Spagnol, *Int. J. Hydrogen Energy*, 2005, **30**, 1297–1302.
4 X. Li and I. Sabir, *Int. J. Hydrogen Energy*, 2005, **30**, 359–371.
5 H. Tawfik, Y. Hung and D. Mahajan, *J. Power Sources*, 2007, **163**, 755–767.
6 E. A. Cho, U. S. Jeon, H. Y. Ha, S. A. Hong and I. H. Oh, *J. Power Sources*, 2004, **125**, 178–182.
7 R. A. Antunes, M. C. L. Oliveira, G. Ett and V. Ett, *Int. J. Hydrogen Energy*, 2010, **35**, 3632–3647.
8 S. Karimi, N. Fraser, B. Roberts and F. R. Foulkes, *Adv. Mater. Sci. Eng.*, 2012, **2012**, 828070.
9 G. Vyas, M. H. Abd Elhamid, Y. M. Mikhail and R. H. Blunk, *US Pat.*, US 7632592 B2, 2009.
10 M. H. Fronk, R. L. Borup, J. S. Hulett, B. K. Brady and K. M. Cunningham, *US Pat.*, US 6372376 B1, 2002.
11 C. Ma, H. Kuan, H. Wu, H. Su, S. Liao, C. Yen, Y. Lin and Y. Cheng, *US Pat.*, US 7910040 B22011.
12 R. Taherian, M. J. Hadianfard and A. N. Golikand, *Mater. Des.*, 2013, **49**, 242–251.
13 C. Shen, M. Pan, Z. Hua and R. Yuan, *J. Power Sources*, 2007, **166**, 419–423.
14 C. Shen, M. Pan, Q. Wu and R. Yuan, *J. Power Sources*, 2006, **159**, 1078–1083.
15 http://www1.eere.energy.gov/hydrogenandfuelcells/mypp/pdfs/fuel_cells.pdf.
16 C. K. Chau, F. Qiao and Z. Li, *Construct. Build. Mater.*, 2011, **25**, 2911–2917.
17 H. Ma, B. Xu, J. Liu, H. Pei and Z. Li, *Mater. Des.*, 2014, **64**, 497–502.
18 B. Xu, H. Ma and Z. Li, *Cem. Concr. Res.*, 2015, **68**, 1–9.
19 H. Ma, B. Xu and Z. Li, *Cem. Concr. Res.*, 2014, **65**, 96–104.
20 C. Gao and G. Chen, *Compos. Sci. Technol.*, 2016, **124**, 52–70.
21 C. Micaela, C. Alessandro, S. M. Imran, J. P. Vitthal and T. Alberto, *Composites, Part A*, 2014, **61**, 108–114.
22 Z. Hu and G. Chen, *Adv. Mater.*, 2014, **26**, 5950–5956.
23 M. C. L. Oliveira, G. Ett and R. A. Antunes, *J. Power Sources*, 2013, **221**, 345–355.
24 H. Fang, C. Liu, C. Liu, F. Li, M. Liu and H. M. Cheng, *Chem. Mater.*, 2004, **16**, 5744–5750.
25 H. Ma, *J. Porous Mater.*, 2014, **21**, 207–215.